ELSEVIER

Physica B 217 (1996) 193–206

PHYSICA B

Confinement and the CLOPW method

H.G. Bekker[a], C.M.J. Wijers[a,*], N.E. Christensen[b]

[a] *Faculty of Applied Physics, Twente University, P.O. Box 217, 7500 AE Enschede, The Netherlands*
[b] *Institute of Physics and Astronomy, Aarhus University, DK-8000 Aarhus C, Denmark*

Received 31 July 1995

Abstract

Plane waves and Confined Localized Orbitals have been used to construct a new mixed basis for electronic structure calculations. Confinement is a mathematical transformation which smoothly suppresses the tails of the atomic orbitals. This eliminates multicentre integrals in the expressions for the matrix elements. Using self-consistent potentials supplied by the linear muffin tin orbital method (LMTO) we have calculated the bulk band structures of Al, Si, Cu, and LiH to a degree of accuracy comparable with the results given by the LMTO calculations. The basis functions are energy independent so the full solution is obtained without invoking any kind of linearization scheme.

1. Introduction

Theoretically, the easiest way to solve the bulk electronic dispersion problem (band structure) is by means of the plane wave (PW) method. The pure PW method however is hampered by a bad convergence behaviour caused by the singularities in the potential introduced by the nuclei. Attempts to cure the PW method concentrate mainly on either modifying the basis to improve convergence or modifying the potential by removing the $1/r$ singularities. These attempts have led to many methods, like the OPW method [1], the APW method [2] and the large family of pseudo-potential methods.

In this paper we will investigate a mixed basis set (MB) approach, using a type of mixed basis set, labeled CLOPW. MB methods augment the PW basis set by addition of localized orbitals. In our case these are *confined* localized orbitals (CLO), which explains the acronym. Analysis of these MB methods [3] has shown a number of potential advantages: an energy-independent basis set and the ability to handle potentials without restricting their shape. However, the addition of localized orbitals of the LCAO-type forces a multitude of multicentre integrals to be evaluated, turning down the numerical efficiency of the method and destroying most of the transparency and simplicity of the original PW method. These multicentre integrals are caused by the tails of the orbitals which extend (in principle) throughout the whole crystal. For this reason Kang et al. [4] have used nonoverlapping localized orbitals. They showed that the efficiency of the resulting method was significantly improved. The same basis set has been used later by Singh [5] for his projector-basis technique. The CLOPW method given in this paper follows similar strategies as to

* Corresponding author.

SSDI 0921-4526(95)00888-8

the basis set, but offers further simplification by using confined localized orbitals.

Confinement removes the tails of the localized orbital part in a mathematically rigourous way while preserving the shape of the localized orbitals near the nuclei. Since the mathematical operation used to do the confinement, contracts the original tight-binding-type localized orbital to within spatially disjunct confinement spheres, it is evident that this will lead (under certain conditions) to the removal of all multicentre integrals in the expressions for the secular matrix elements. We will further show that the tails can be removed without introducing APW-like discontinuities in the basis functions or their derivatives. In practice, some kind of overlap is allowed and improves convergence. Confinement is a general technique and can be applied equally well to any type of localized orbital being square integrable. In our method we have confined tight binding orbitals composed of hydrogenic states to augment the basis set. These have the advantages of being analytic functions and being solutions to a Z/r potential making them more efficient in the representation of low-lying core states than Gaussian orbitals. In the present paper we calculate a number of classical band structure problems to test the choice of the basis set itself. The problems have been selected to demonstrate the versatility of the method.

One of the main objectives to develop the method has been the calculation of cellular quantities. By cellular quantity we mean the expectation value of some operator calculated over a subregion (cell) of the total region for which we have solved the Schrödinger equation. An example in the field of optics: We define a cell containing a single atom, somewhere inside a solid. This cell is of the Wigner–Seitz type and we want to know its local polarizability. In a previous publication [6] we have given an expression for this kind of cellular quantity α_k:

$$\overleftrightarrow{\alpha}_k(\omega) = \frac{e^2}{\hbar}\sum_i\sum_f \langle\phi_i|\boldsymbol{r}|\phi_f\rangle_{\Omega_k}\langle\phi_i|\boldsymbol{r}|\phi_f\rangle^{\mathrm{T}*}_{\Omega_k}\hat{F}_{if}(\omega), \quad (1)$$

where Ω_k indicates the kth cell, ϕ_i, ϕ_f are initial and final states and $\hat{F}_{if}(\omega)$ is a frequency-dependent factor. For complicated (surface) optical problems these local polarizabilities are indispensable, but not easy to calculate. Using a CLOPW basis set the expectation value of $\boldsymbol{r}$ splits into three parts: CLO–CLO, CLO–PW and PW–PW. As long as the confinement sphere is inside the cell, the matrix elements between two CLO's and a CLO and a PW reduce to simple one-dimensional integrals. The real problem is the surface of the cell. This surface however consists of a few plane segments, intersected only by the PW's which turns out to be mathematically convenient.

Other applications of the CLOPW basis set can be sought in the field of structure optimizations where one needs to calculate the forces working on atoms. Hellmann and Feynman showed how these forces should in principle be calculated [7]. Later on it has been shown [8] that in general the HF force has to be corrected for the effects of the incomplete basis set (IBS) used in the electronic structure calculation. For the LAPW basis the IBS corrections have been worked out by Yu et al. [9]. Similar results can be obtained by means of the CLOPW method, by deriving the IBS corrections in a way analogous to the Yu LAPW derivation. The simpler and more straightforward character of the CLOPW basis set is expected to yield here better expressions for the atomic force.

The remaining part of the paper is organized as follows: The confinement transformation is discussed in Section 2. In Section 3 we present the expressions for the basis functions and the matrix elements of the secular equation. In Section 4 we present some band structure calculations which we compare to the band structures given by the linear muffin tin orbital (LMTO) method [11] *using the same self-consistent potential.* Finally, we summarise our findings and present our conclusions in Section 5.

2. Confinement operators

As mentioned already in the introduction the starting point of the CLOPW method are spherically symmetric orbitals Ψ, written as

$$\Psi_{nlm}(r, \theta, \phi) = R_{nl}(r)\,Y_{lm}(\theta, \phi), \quad (2)$$

where r is in spherical coordinates (r, θ, ϕ). The Y_{lm}'s are the usual spherical harmonics. In the calculations we have used for $R_{nl}(r)$ hydrogenic orbitals as given in Ref. [10].

Given an arbitrary (complex) function $\phi(r)$, confinement can be defined in general as an operator $\mathscr{C}$, which should obey the following set of rules:

$$\mathscr{C}(\phi(r)) \sim \phi(r) \quad \text{for } |r - R| \to 0, \quad R\text{: lattice site},$$

$$\mathscr{C}(\phi(r)) = 0 \quad \text{for } |r - R| > R_c,$$

$$\frac{d^n}{dr^n}\mathscr{C}(\phi(r)) = 0 \quad \text{for } |r - R| = R_c \text{ and } n = 1, 2 \text{ (at least)},$$

where R_c is the confinement radius, determining the size of the confinement sphere. These confinement spheres should be nonoverlapping between neighbouring sites. The construction of the confinement operator is not unique. In this paper two types of confinement, implicit and enveloped will be discussed, both obeying the requirements given above.

2.1. Implicit confinement

For implicit confinement, primarily the radial coordinate r has to be taken into account. The way this coordinate shows up in Ref. [2], is as an unconfined coordinate. For the case of implicit confinement, it cannot be used as such and the notation will be changed from r to $\tilde{r}$. What is going to be used in the basis set (CLO-part) is the confined coordinate r and this gives the confinement operator $\mathscr{C}$ as

$$\mathscr{C}(\phi(r)) = \phi(\tilde{r}(r), \hat{r}). \tag{3}$$

There is a large degree of freedom to select an implicit confinement $\tilde{r}(r)$. An elegant choice is the tangent:

$$\tilde{r}(r) = \tan\left(\frac{\pi r}{2R_c}\right). \tag{4}$$

The following choice has been used by us and contains only basic algebraic operations:

$$\tilde{r}(r) = \frac{r}{1 - (r/R_c)^{n_c}}, \tag{5}$$

where R_c is the confinement radius and n_c is the confinement order. The amount of "distortion" of the original wave function is determined by those two parameters. The higher the confinement order n_c the larger the volume of the confinement sphere, where the confined solution approximates the original solution. It is however not advantageous to use too high values for it, as we will show later on. In practice, values of 2 or 3 are optimal. Implicit confinement causes the nodes to shift.

2.2. Enveloped confinement

Enveloped confinement works differently. It meets the general requirements, by multiplying the radial solutions with a suitably chosen envelope function. Confinement within the envelope approach, depends completely on this envelope function $f(r)$:

$$\mathscr{C}(\phi(r)) = f(r)\phi(r). \tag{6}$$

The main point is the construction of $f(r)$. Our approach has been to select a simple function being 1 near the origin and going smoothly to 0 at infinity. To such a function we apply the implicit confinement $\tilde{r}(r)$, given by Eq. (5). Gaussians are useful for enveloped confinement:

$$f(\tilde{r}) = e^{-\tilde{r}^2}, \tag{7}$$

but we prefer the Lorentzian:

$$f(\tilde{r}) = \frac{1}{1 + \tilde{r}^2}, \tag{8}$$

since it contains only simple algebraic operations. The advantage of enveloped confinement, is that the positions of the nodes of the confined functions remain unchanged. The disadvantage is that the expressions for the matrix elements become more complex, than for implicit confinement.

2.3. The effect of confinement

By means of some elementary calculations, we show in this section how the different types of confinement behave in practice. Some typical results are shown in Fig. 1. There we have collected

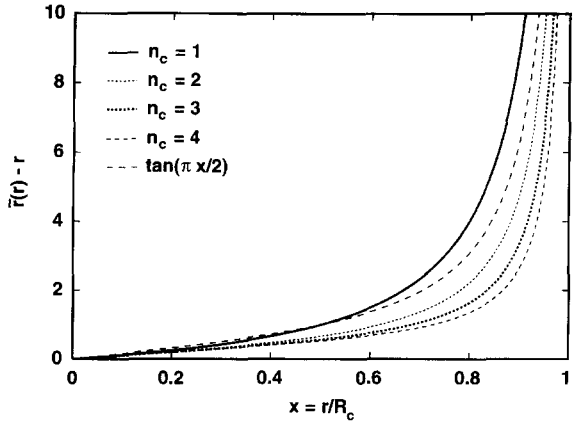

Fig. 1. Implicit confinement $\tilde{r}(r) = r/(1-(r/R_c)^{n_c})$ for confinement orders $n_c = 1, 2, 3, 4$ and $\tilde{r}(r) = \tan(\pi r/2R_c)$ shown as the difference $\tilde{r}(r) - r$.

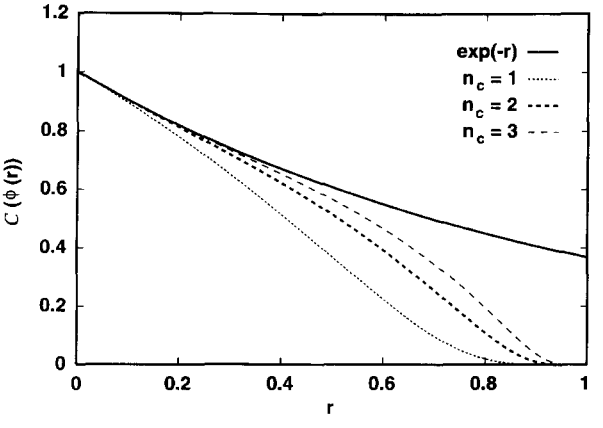

Fig. 2. Implicit confinement of 1s-like orbital e^{-r}, using Eq. (5), for confinement orders $n_c = 1, 2, 3$ and $R_c = 1$.

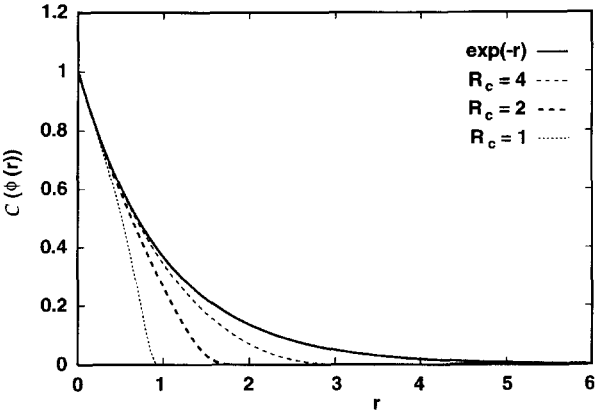

Fig. 3. Implicit confinement of 1s-like orbital e^{-r}, using Eq. (5), for confinement radii $R_c = 1, 2, 4$ and $n_c = 2$.

results for implicit confinement using $R_c = 1.0$. To make the linearity interval more apparent we have plotted $\tilde{r}(r) - r$. It is clear that this interval increases for increasing confinement order n_c, but that there is not much improvement after $n_c = 3$. Further the tan-type of confinement is somewhere in between the confinements with $n_c = 1$ and $n_c = 2$.

Characteristic for all types of implicit confinement, is the occurrence of the singularity near R_c. This singularity causes the infinite range of the unconfined coordinate, as required by the original orbital. The easiest kind of hydrogenic orbital is 1s-like and we show this orbital and its confined counterparts in Fig. 2. Again it can be seen that the confined orbital approximates the original near the origin over a larger interval, when the confinement order n_c increases from 1 to 3. The price is a higher distortion near the confinement radius R_c, which has been kept at a constant value of 1 in this figure.

The other parameter governing the behaviour of confinement and actually the more important one is the confinement radius R_c. Its influence upon the same 1s-like orbital is shown in Fig. 3, for a confinement order $n_c = 2$. Here we see that the higher R_c, the less the distortion becomes both near the origin and near R_c. This would indicate that we want to maximize this parameter without causing overlap between adjacent confinement spheres. One should further take into account the ratio between R_c and na_0/Z when choosing different confinement radii on different atoms.

To conclude this section we show the comparison between implicit types of confinement and enveloped ones for $n_c = 2$ and $R_c = 2$. In Fig. 4, we show the 3p-like orbital $(r - r^2)e^{-r}$, using for the implicit confinement equation (5), and for the enveloped confinement the Lorentzian equation (8), confined by again transformation equation (5). The choice for a 3p-like orbital has been made to demonstrate the influence upon nodes, outside the origin. Both confined orbitals are contracted to

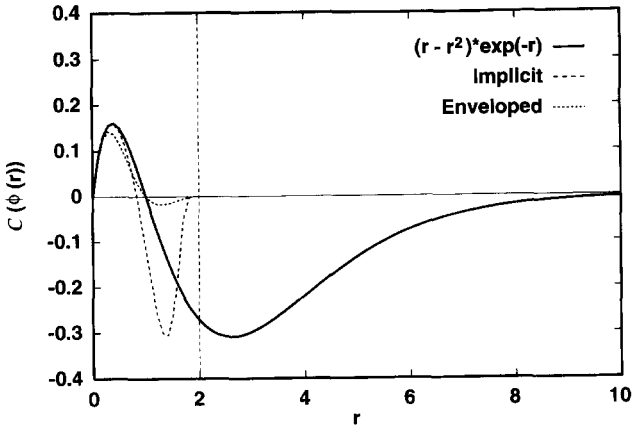

Fig. 4. Comparison of implicit and enveloped confinement of a 3p-like orbital $(r - r^2)e^{-r}$, using for implicit Eq. (5) and for enveloped the Lorentzian Eq. (8). Both with $n_c = 2$ and $R_c = 2$.

within the confinement radius $R_c = 2$. Implicit confinement shifts the nodes, but extrema remain unaffected. Enveloped confinement leaves the nodes exactly at the original positions, but strongly modifies the extrema of the orbital.

Mainly due to the fact that enveloped confinement gives more complicated expressions for virtually all matrix elements in the secular equation, we have concentrated primarily upon implicit confinement. The few tests we have done to investigate enveloped confinement, seem to indicate that both types of confinement behave identical in practice. For the remainder of this paper we will use implicit confinement only.

3. Basis set and matrix elements

All mixed basis sets have plane waves as their common feature:

$$|\boldsymbol{g}\rangle = \phi_{\boldsymbol{g}}(\boldsymbol{k}, \boldsymbol{r}) = \frac{1}{\sqrt{V_{\mathrm{ws}}}} e^{i(\boldsymbol{k}+\boldsymbol{g})\boldsymbol{r}}, \tag{9}$$

where V_{ws} is the volume of the Wigner–Seitz cell. The second part is in our case made up by the confined localized orbitals (CLO), which we define by the Bloch sum:

$$|nlm\boldsymbol{q}\rangle = \phi_{nlm}(\boldsymbol{k}, \boldsymbol{r} - \boldsymbol{q}) = \sum_{\boldsymbol{R}} e^{i\boldsymbol{k}\boldsymbol{R}} \tilde{\phi}_{nlm}(\boldsymbol{r} - \boldsymbol{R} - \boldsymbol{q}), \tag{10}$$

where for $\tilde{\phi}_{nlm}(\boldsymbol{r})$ are chosen in this paper the confined hydrogenic solutions [10]. The $\boldsymbol{R}$ are the sites of the lattice and the $\boldsymbol{q}$ the position of an atom within the Bravais unit cell. It is easy to see that this sum obeys the Bloch criterion.

The overlap matrix is not diagonal so we need both Hamiltonian matrix elements $\langle i|H|j\rangle$ and overlap matrix elements $\langle i|j\rangle$. These two types of matrix elements occur as PW–PW, CLO–PW and CLO–CLO, so we need in total six different expressions for matrix elements. The full derivation of these matrix elements can be found in the appendix. Here we only present the results.

We start with the overlap matrix elements. The PW–PW-type overlap matrix elements are given by the orthonormality of the plane waves:

$$\langle \boldsymbol{g}_i|\boldsymbol{g}_j\rangle = \delta_{ij}. \tag{11}$$

Confinement affects only the radial part of the hydrogenic orbitals so we can still use the orthonormality of the Y_{lm}'s in the evaluation of the CLO–CLO overlap elements

$$\langle nlm\boldsymbol{q}|n'l'm'\boldsymbol{q}\rangle = \int_0^{R_c} \tilde{R}_{nl}(r)\,\tilde{R}_{n'l}(r) r^2\,\mathrm{d}r\,\delta_{ll',mm'}, \tag{12}$$

where the functions $\tilde{R}_{nl}(r)$ are the radial parts of the $\tilde{\phi}_{nlm}(\boldsymbol{r})$. The same orthonormality can be used for the overlap matrix elements between plane waves

and CLO's

$$\langle nlmq|k+g\rangle = e^{i(k+g)q}\frac{4\pi}{\sqrt{V_{ws}}} i^l Y^*_{lm}(\widehat{k+g}) \times \int_0^{R_c} j_l(|k+g|r)\,\tilde{R}_{nl}(r) r^2\,dr. \quad (13)$$

The plane wave has been expanded in spherical Bessel functions. Note that the integrals run from the origin to the sphere radius of the confinement sphere positioned at q.

Within the effective one electron description, the crystal Hamiltonian is written as (Hartree atomic units)

$$H = -\frac{\nabla^2}{2} + V(r), \quad (14)$$

where $V(r)$ is the effective one electron potential. We start the derivation of the Hamiltonian matrix elements with the PW–PW elements. This matrix element is given as

$$\langle g_i|H|g_j\rangle = \frac{|k+g_i|^2}{2}\delta_{ij} + \frac{1}{V_{ws}}\int_{V_{ws}} V(r)e^{i(g_j-g_i)r}\,dr. \quad (15)$$

We will derive in Section 3.3 the final form of this matrix element.

In the derivation of the following matrix elements we assume that the potential is spherically symmetric inside the confinement sphere. The CLO–CLO part of the Hamiltonian matrix elements makes again use of the orthonormality of the Y_{lm}'s. The following highly symmetric expression can be obtained:

$$\langle nlmq|H|n'l'm'q\rangle = \int_0^{R_c}\left[\frac{1}{2}\left[\left(\frac{d\tilde{R}_{nl}(r)}{dr}\right)\left(\frac{d\tilde{R}_{n'l}(r)}{dr}\right)r^2 + l(l+1)\tilde{R}_{nl}(r)\tilde{R}_{n'l}(r)\right] + V(r)r^2\tilde{R}_{nl}(r)\tilde{R}_{n'l}(r)\right]dr\,\delta_{ll',mm'}. \quad (16)$$

Note that $\tilde{R}_{nl}(r)$ and its derivatives are analytic functions. There is no need for numerical differentiations in the calculation of these matrix elements.

The final matrix element is the CLO–PW Hamiltonian matrix element given by

$$\langle nlmq|H|k+g\rangle = e^{i(k+g)q}\frac{4\pi}{\sqrt{V_{ws}}} i^l Y^*_{lm}(\widehat{k+g})\int_0^{R_c} j_l(|k+g|r)\tilde{R}_{nl}(r) \times\left[\frac{|k+g|^2}{2} + V(r)\right]r^2\,dr. \quad (17)$$

All integrals appearing in the CLO–CLO and CLO–PW-type matrix elements are one dimensional. The $\langle g_i|V(r)|g_j\rangle$ element (15) is the only matrix element containing a full three-dimensional integral, but this is simply the Fourier coefficient of the potential. For a muffin tin potential an efficient method exists to evaluate these coefficients.

3.1. Behaviour matrix elements

Most of the behaviour of the confined orbitals has been explained already in Section 2.3. Further influence relates to the behaviour of the matrix elements and shows up in the orthogonality of the set and the radial derivative, occurring in the kinetic energy part of the matrix elements.

The overlap matrix elements between CLOPW-type basis functions, show the orthogonality of the set. In the limit for R_c to ∞ the CLO–CLO matrix elements show perfect orthonormality. This orthonormality disappears for decreasing R_c. The higher n_c, the slower orthonormality disappears for smaller R_c. This is as expected from the behaviour of confinement.

The more interesting matrix element with respect to orthogonality, is the matrix element between CLO's and plane waves. These matrix elements approach a constant nonzero value for R_c going to ∞, independently from the value of n_c. For $n_c = 1$ we have found a monotonously increasing $\langle 2p_0|(0,0,1)\rangle$ matrix element. For all higher values of n_c a maximum is found. In the orthogonality checks the CLO's have not been (re)normalized under confinement.

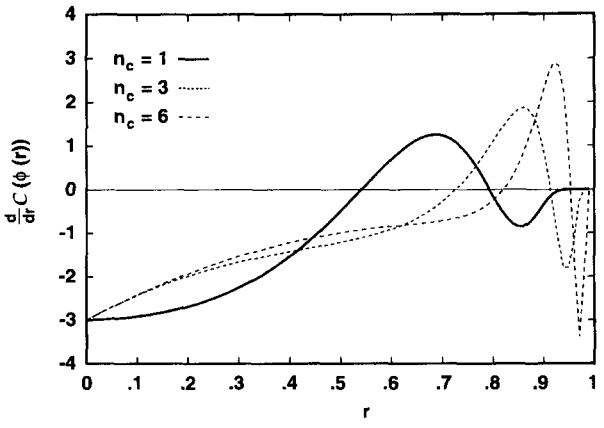

Fig. 5. Radial derivative for a 3s-like orbital, $R_c = 1.0$ and $n_c = 1, 3, 6$.

For the last phenomenon, related to confinement, one has to take a closer look at Eq. (16). This is the only matrix element directly depending on the value of the derivative of $\tilde{R}_{nl}(r)$. We have shown this derivative in Fig. 5 for the 3s-like orbital (unconfined) $f(r) = (-3 + (10/3)r - (2/3)r^2)\exp(-r)$. For a confinement radius $R_c = 1.0$ we show the derivative for values of $n_c = 1, 3, 6$. We see that for this choice of parameters, higher and higher values of the derivative occur near R_c, if n_c increases. These oscillations can cause problems. They have the tendency to introduce sharp variations in the wave function. Those need to be compensated by the variational procedure, but at the expense of a large number of plane waves. In practice this influence almost completely disappears for large values of Z, but only if the values for the quantum numbers *nlm* remain low. Increasing those values too, causes again stronger oscillations. Since these oscillations affect the Hamiltonian matrix element through the kinetic energy part, we like to call them "kinetic ripples". Letting n_c go to ∞, will cause the ripples to become very strong and sharp in a very small interval near R_c. This effect shows analogy to the kinetic energy contribution of the muffin tin sphere surface in the APW method, where the singular behaviour of this surface cannot be neglected.

The CLOPW basis set as such is overcomplete, but for actual calculations always a limited subset will be selected, being undercomplete. The selection of the CLO part is critical. Enough of these CLO basis functions have to be selected in order to compensate for the influence of the nuclei, but there is an upper limit. If CLO's with too high quantum numbers, particularly n, have to be invoked, the "kinetic ripples" start to become a serious problem and as a result the calculated energy values start to deteriorate.

We have found the following as a rule of thumb for the number of CLO's in the basis: per unit cell atom, the set of CLO's, corresponding with the occupied states of the isolated atom. Optionally, the CLO's corresponding to the first unoccupied (isolated atom) levels can be added to the basis.

3.2. Constructing the potential

We shall not here describe the results of self-consistent calculations, but rather we will illustrate the accuracy of the method by applying it together with the LMTO method to the test cases using the same potential.

The external self-consistent potential we have used for our calculations is defined in the so-called atomic sphere approximation (ASA) [11]. The Wigner–Seitz cell is filled up with spheres which in general are overlapping. Inside these spheres the ASA potential is defined to be spherically symmetric. For the CLOPW method we have to transform this ASA potential to muffin tin shape, by defining inside the ASA spheres smaller muffin tin spheres. The muffin tin sphere radii are chosen such that they are touching. Outside the muffin tin spheres we define the muffin tin zero as

$$V_{mtz} = \frac{\sum_q S_q^2 V_{\mathrm{ASA}}(S_q)}{\sum_q S_q^2}. \tag{18}$$

Here S_q are the radii of the ASA spheres, where the vector $\boldsymbol{q}$, defined before, gives the position of that ASA/muffin tin sphere within the unit cell. Inside the muffin tin sphere the muffin tin potential is equal to the ASA potential. We will show in the next section that this construction of the potential gives reasonable results for monoatomic close-packed metals like Al and Cu but that the results are less satisfying for materials like Si or LiH with multiple atoms in the conventional unit cell. It

turned out that in some cases the muffin tin spheres had to be increased to the size of the ASA spheres to get an accurate description of the potential in the interstitial region. Any effects of the overlap between the muffin tin spheres were ignored in these cases.

The Fourier components of the muffin tin potential can be calculated in the following way:

$$\langle \boldsymbol{g}|V(r)|\boldsymbol{g}'\rangle = \sum_q \int_{S_q} V(|\boldsymbol{r}-\boldsymbol{q}|)e^{i(\boldsymbol{g}'-\boldsymbol{g})\boldsymbol{r}}\,d\boldsymbol{r} + \int_I V_{mtz}\,e^{i(\boldsymbol{g}'-\boldsymbol{g})\boldsymbol{r}}\,d\boldsymbol{r}. \tag{19}$$

The first integral on the right-hand side is over a muffin tin sphere. The second integral is over the interstitial region I. The sum runs over all muffin tin spheres. Now if we replace the term $V(r)$ in the first integral by $V(r) + V_{mtz} - V_{mtz}$ we can rewrite these integrations as

$$\langle \boldsymbol{g}|V(r)|\boldsymbol{g}'\rangle = \frac{1}{V_{\mathrm{ws}}}\left[\sum_q \int_{S_q} (V(|\boldsymbol{r}-\boldsymbol{q}|) - V_{mtz})e^{i(\boldsymbol{g}'-\boldsymbol{g})\boldsymbol{r}}\,d\boldsymbol{r} + \int_{V_{\mathrm{ws}}} V_{mtz}\,e^{i(\boldsymbol{g}'-\boldsymbol{g})\boldsymbol{r}}\,d\boldsymbol{r}\right]. \tag{20}$$

Using the expansion of plane waves into spherical harmonics (A.1) we end up with the following expression for the Fourier components:

$$\langle \boldsymbol{g}|V(r)|\boldsymbol{g}'\rangle = \frac{1}{V_{\mathrm{ws}}}\sum_q e^{i(\boldsymbol{g}'-\boldsymbol{g})\boldsymbol{q}} \times \int_0^{(R_c)_q} (V(r) - V_{mtz})j_0(|\boldsymbol{g}'-\boldsymbol{g}|r)r^2\,dr + V_{mtz}\delta_{ij}. \tag{21}$$

This expression has been used as the potential part of Eq. (15).

4. Calculations

In this section we present a selection of band structures calculated by the CLOPW method using the modified LMTO-ASA potential. We will compare the CLOPW results for the materials Al, Si, Cu, and LiH with the results from the original LMTO-ASA calculation, which supplied the self-consistent potential. Al has been selected as the classical nearly free electron material. Si has been studied to investigate materials with covalent bonding and also because it is so well-documented. Cu has been chosen to demonstrate the capability of the CLOPW-method to deal with d-band states. LiH has been taken for a couple of reasons. It is an ionic material, it is a compound and it contains hydrogen.

Note that all calculations have been performed without a frozen core approximation. All core and valence eigen energies lie in one energy panel and we solve the all electron problem for each k-point separately. This has the advantage that possible hybridizations of higher core states among themselves or with valence states will be correctly described.

Unless stated otherwise we will take for the parameter Z of the CLO's the atomic number of the atom on which this CLO is centred. Energies will be given with respect to the bottom of the valence band (Γ_1 state). For one case (Si) we will show the convergence behaviour.

4.1. Aluminum

The first material we will focus upon, is Al in the fcc structure. We have performed the calculations with 9 CLO's and a cut-off energy of 120 eV for the plane waves (59 plane waves). For this basis the valence eigenvalues had converged to within 0.1 eV. The confinement radius was 2.7 a.u. which is also the muffin tin sphere radius. For the FCC lattice parameter we took 7.653 a.u.

The calculated CLOPW band structure along a few high-symmetry lines in the IBZ is shown in Fig. 6. For the high-symmetry points X, L and W we have given in Table 1 numerical values for the energy. We have found the Fermi-level to be at 11.1561 eV (relative to the Γ_1 state). The agreement between the CLOPW-type of results and the LMTO-ASA derived ones is very good and deviates typically not larger than 0.1 eV, whereas near E_F agreement can be found at a 0.01 eV level. More

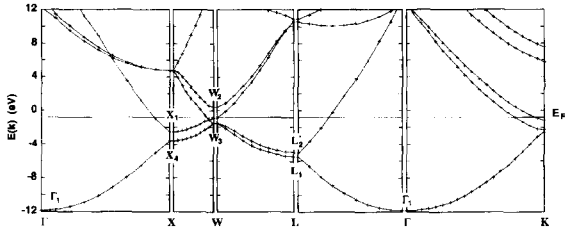

Fig. 6. Band structure of Al.

Table 1
Band energies for Al at selected high-symmetry points

	I	II	(II–I)
X_1	9.38	9.36	−0.02
X_4	8.27	8.38	+0.11
L_1	6.39	6.50	+0.11
L_2'	6.87	6.78	−0.09
W_3	10.35	10.45	+0.10
W_2'	12.32	12.33	+0.01

All energies (in eV) have been taken relative to the Γ_1 state. Column I: CLOPW calculation. Column II: LMTO-ASA calculation.

accurate statistical analysis of those data learns that the average deviation for LMTO-ASA is 0.037 eV, with a standard deviation of 0.083 eV. The distance between the two L-levels (L_1, L_2') has been obtained by Snow [12] as 0.33 eV and Faulkner [13] as 0.47 eV. The first used an APW calculation with a model potential and the second a KKR-calculation. We found for the distance between the two L-levels 0.48 eV for CLOPW and 0.28 eV for the LMTO-ASA. Those values compare well with the Snow and Faulkner calculations. The difference between the CLOPW and LMTO-ASA calculations are probably caused by the muffin tin modifications we made to the LMTO-ASA potential. There is a singnificant difference between the atomic sphere radius (2.90 a.u.) and the muffin tin sphere radius (2.7 a.u.) (see Section 3.2).

As we performed an all-electron calculation it is instructive to see how the core states behave compared to the numerical solutions of the radial Schrödinger equation. As a representative case we show in Fig. 7 the 2s core function in Al together

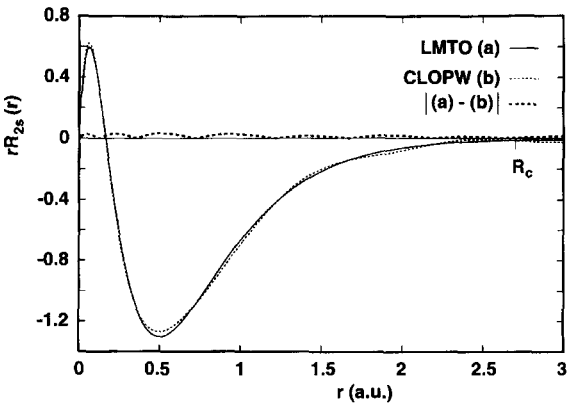

Fig. 7. Radial part $rR_{2s}(r)$ of the 2s core state of Al as a function of r (a.u.). (a): LMTO calculation, (b): CLOPW calculation. Fat dashed curve: absolute difference of (a) and (b). $R_c = 2.7$ a.u.

with the numerical solution of the radial Schrödinger equation. For a cut-off energy of 120 eV we obtained for the eigen energy from the CLOPW calculation −101.31 eV. The energy found by the numerical integration was −102.86 eV. For a cut-off energy of 500 eV we calculated an eigen energy of −102.27 eV

4.2. Copper

The second material, we have investigated to test the CLOPW method, is Cu. Here we used 46 CLO's and a cut-off energy of 250 eV (1 1 3 plane waves). The convergence of the band energies is within 0.1 eV. For the confinement radius we took 2.8 a.u. which is larger than the radius for touching spheres of 2.41 a.u. The oversized confinement spheres did not influence results, the confined orbitals were typically of the order $O(10^{-8})$ in the overlap region, but allowed for a smaller basis set. We took for the FCC lattice parameter 6.82 a.u.

We show the CLOPW calculated band structure for this metal in Fig. 8 and in Table 2 we show some band energies on selected high-symmetry points. There is a remarkable difference for Cu with respect Al. Deviations between LMTO-ASA and CLOPW obtained results for Al have random sign, whereas the corresponding deviations for Cu are systematically positive. It turns out that LMTO-ASA produces higher energies, in average 0.063 eV for the

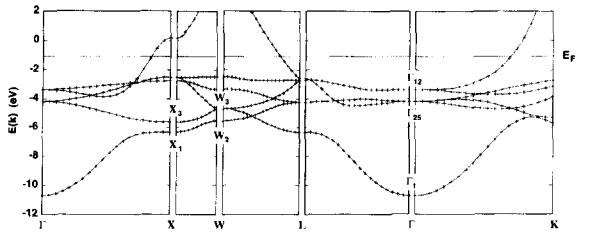

Fig. 8. Band structure of Cu.

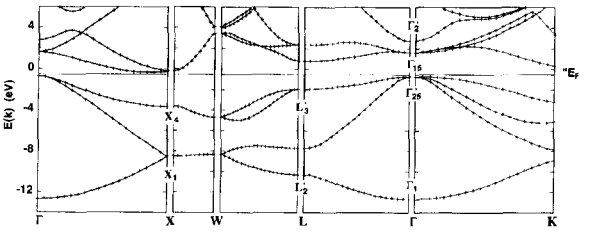

Fig. 9. Band structure of Si.

Table 2
Band energies for Cu at selected high-symmetry points

	I	II	(II–I)
Γ'_{25}	6.51	6.56	+ 0.05
Γ_{12}	7.35	7.37	+ 0.02
X_1	4.39	4.50	+ 0.11
X_3	5.09	5.14	+ 0.05
W_2	5.18	5.29	+ 0.11
W_3	6.01	6.05	+ 0.04

All energies (in eV) have been taken relative to the Γ_1 state. Column I: CLOPW calculation. Column II: LMTO-ASA calculation.

points given, with a standard deviation of 0.038 eV. For the comparison between CLOPW and LMTO-ASA, we find the stronger deviations at X_1, W_2 (0.11 eV), but the nearby levels X_3, W_3 deviate no more but 0.05 eV, so we do not see reasons to ascribe the systematic deviations to the influence of the d-band states. The systematic part of the deviation has to be due to the muffin tin modification of the LMTO-ASA potential.

For a number of cases we also focussed on the bandwidth of the lowest band, where we used the distance between the Γ_1 and X_1 level. This bandwidth is 4.39 eV for the CLOPW method and 4.50 eV for the LMTO-ASA method. Modrak [14] finds a smaller bandwidth of 4.15 eV. The old calculations of Burdick [15] yield a value of 3.58 eV. A later publication of Takeda and Kübler [16] gives 4.93 eV. The CLOPW- and LMTO-ASA results are well within the limits given by other methods which use muffin-tin-type potentials.

For copper we have found the Fermi-level to be at 9.594 eV.

4.3. Silicon

Next we calculated the band structure for Si, the classical example of covalent bonding in solids. We used 23 CLO's per atom and a cut-off energy of 120 eV (113 plane waves). The eigen energies are converged to within 0.1 eV. For the confinement radius we took $R_c = 2.53$ a.u. the ASA radius. This is larger than the radius for touching spheres (2.22 a.u.), but the values of the CLO's at this radius were of the order $O(10^{-7})$, making the overlap negligible.

In the construction of the potential we had to increase the muffin tin radius to the value of the ASA radius (2.53 a.u.). Using the muffin tin radius for touching spheres (2.22 a.u.), we found a band structure without a band gap. This is a strong indication that the shape of the valence and conduction bands is very sensitive to the potential in the region in between the two silicon atoms in the unit cell. If we use a small muffin tin radius a vital part of the potential in this region is averaged out in the muffin tin zero. By taking overlapping muffin tin spheres we introduce also errors in the Fourier coefficients of the potential (see Section 3.2). These errors will particularly affect the excited states.

The calculated band structure is shown in Fig. 9 and numerical values for energies at some selected points in the IBZ in Table 3. The horizontal line marked "E_F" is just an auxiliary line in the middle of the gap, to facilitate distinction between occupied and unoccupied bands. The differences between the CLOPW calculation and the two reference calculations is again given in this table. The deviation between the CLOPW- and LMTO-ASA calculation is in average 0.036 eV for the seven selected points and the scatter in these deviations is

Table 3
Band energies for Si at selected high-symmetry points

	I	II	(II–I)
Γ'_{25}	11.99	12.03	+ 0.04
Γ_{15}	14.33	14.72	+ 0.39
Γ'_2	15.46	15.14	− 0.32
X_1	4.18	4.13	− 0.05
X_4	9.03	9.15	+ 0.12
L'_2	2.37	2.32	− 0.05
L'_3	10.75	10.87	+ 0.12

All energies (in eV) have been taken relative to the Γ_1 state. Column 1: CLOPW calculation. Column 2: LMTO-ASA calculation.

Table 4

	I	II
Γ'_{25}	12.31	0.32
Γ_{15}	14.20	− 0.13
Γ'_2	15.24	− 0.22
X_1	4.27	0.09
X_4	9.11	0.08

Column I: CLOPW Band energies (in eV) for Si at selected high symmetry points relative to the Γ_1 state. Calculation with touching muffin tin spheres. Column II: difference between column I and column I of Table 3.

0.22 eV. We have found a bandgap E_G for Si of 0.37 eV, compared to the bandgap of 0.64 eV found by the LMTO-ASA calculation. In contrast to the two previous cases the large discrepancies are now found at Γ.

To illustrate the effect the choice of the muffin tin radius has on the eigenvalues we show in Table 4 the same eigenvalues as in Table 3, but now for a muffin tin radius of 2.22 a.u. (touching spheres). Clearly small deviations in the muffin tin radius have a large influence on particularly the distance between valence and conduction bands.

For Si, we have also investigated explicitly the convergence behaviour. The results are shown in Table 5. The convergence has been tested by varying the number of plane waves, keeping the CLO part of the basis set fixed. The table gives the number of plane waves, having a free electron energy below the cut-off energy E_c. It is clear that

Table 5
Convergence of Silicon band energies (in eV) at selected high-symmetry points

E_c (eV)	180	120	60
# PW	279	113	51
Γ'_{25}	11.98	11.99	12.18
Γ_{15}	14.32	14.33	14.61
Γ'_2	15.43	15.46	15.47

already for 113 plane waves convergence is achieved below 0.1 eV. We see from the convergence behaviour that in particular the Γ_{15} state has a significant PW contribution. Therefore, the previously mentioned errors in the Fourier coefficients of the muffin tin potential have a relatively strong effect on the energy of this state.

Finally, we have calculated for Si the valence charge density in the (1 1 0)-plane as shown in Fig. 10. These results are in good agreement with those obtained by Andersen et al. [17]. Especially, the double maximum found in the bonding region is reproduced well.

4.4. Lithium hydride

As a final example we calculated the band structure of LiH in the Rocksalt structure. We used one 1s CLO on the H atom, two CLO's (1s and 2s) on the Li atom and a cut-off energy of 250 eV (1 6 9 plane waves). For the confinement radii we took $R_c = 1.89$ a.u. for CLO's centred on the Li atom and $R_c = 0.7$ a.u. for the CLO centred on the H atom. For the lattice parameter has been used $a = 7.71$ a.u.

The band structure can be found in Fig. 11 and band energies for some selected high-symmetry points in the IBZ in Table 6.

There are some significant differences between the CLOPW and the LMTO-ASA results. Because of the use of the muffin tin potential the CLOPW method could not be used in the most efficient way. In principle, the confinement sphere on Li could have a radius $R_c = 3.16$ a.u. to make it touch the confinement sphere on the nearest-neighbour atoms (hydrogen). However in the present scheme,

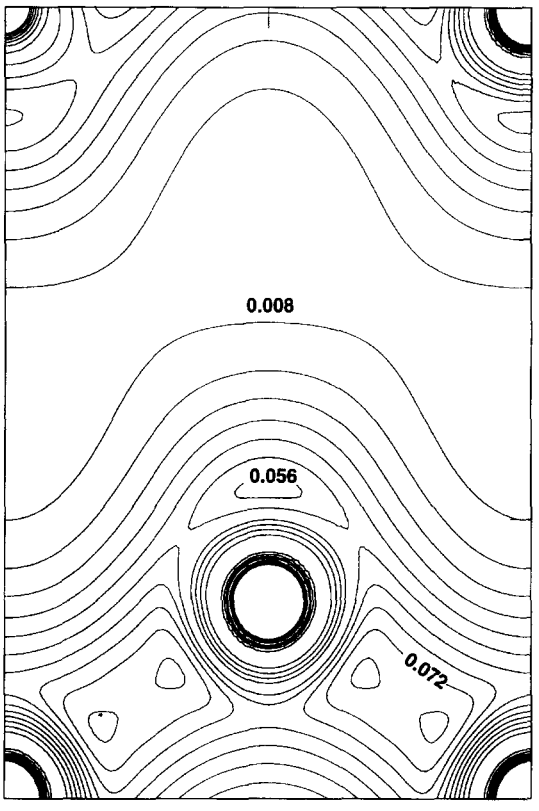

Fig. 10. Valence charge density of Si in the (1 1 0) plane.

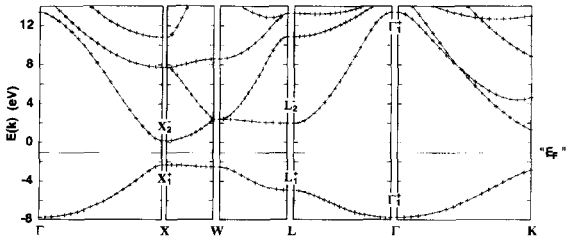

Fig. 11. Band structure of LiH.

we cannot increase our confinement radius beyond the ASA radius (1.90 a.u.).

Previous calculations on Al, Cu, and Si have shown that decreasing the size of confinement spheres below their maximum value (nonoverlapping spheres) always deteriorates the results. We found however that for the present calculation we could safely reduce the confinement sphere of the 1s

Table 6
Band energies (in eV) for LiH at selected high-symmetry points. Eigenvalues for a muffin tin radius of 2.22 a.u.

	I	II	(II–I)
Γ_1^+	21.13	21.06	−0.07
L_1^+	2.82	2.76	−0.05
L_2^-	9.78	9.97	−0.06
X_1^+	5.49	5.35	−0.14
X_2^-	7.97	8.09	+0.12

All energies have been taken relative to the Γ_1 state. Column I: CLOPW calculation. Column II: LMTO-ASA calculation.

CLO centred on the H atom to a radius of 0.7 a.u. not affecting significantly (> 0.001 eV) the eigen energies. Decreasing the confinement sphere centred on Li did have a negative influence on the convergence of the eigenvalues as a function of the number of plane waves. This suggests that the ratio of confinement spheres should be close to the ratio of the effective sizes of the atoms in the compound, with the largest confinement sphere on the big atom.

In the present calculation the relatively small radius for the confinement sphere on Li means that the CLO's centred on Li are "bunched up" inside the confinement sphere and loose some of their efficiency. This has to be compensated by adding more plane waves to the basis, ending up with the slow convergence typical for a plane wave basis. We therefore expect that CLOPW will perform much better with a potential which does not restrict the sizes of the confinement spheres.

5. Conclusions

In this paper we have investigated a new mixed basis: CLOPW. The band structures we calculated for Al, Cu, Si, and LiH are in good agreement with the results given by the LMTO-ASA calculations which supplied the self-consistent potentials. The main cause for the deviation between the two methods is the modification of the ASA potential into a muffin tin potential.

There are however no inherent limitations posed on the form of the potential by the CLOPW

method and we hope to publish a self-consistent full potental version of CLOPW in the near future.

Acknowledgements

One of us (CW) wishes to thank J.P.A. van der Wagt for fruitful and inspiring discussions during the early stages of development of the CLOPW method. We would also like to thank P.L. de Boeij, W.W. Schulz, and A. Svane for their constructive criticism and valuable advice.

Appendix: Derivation matrix elements

In this appendix the derivation of the expressions for the matrix elements will be given, apart from the PW–PW-type of matrix elements, and the CLO–CLO overlap matrix element, those being trivial. To evaluate the CLO–PW-type matrix elements we need the well-known expansion of plane waves into spherical harmonics:

$$e^{i\boldsymbol{k}\boldsymbol{r}} = 4\pi \sum_{l=0}^{\infty} i^l \sum_{m=-l}^{l} j_l(kr)\, Y^*_{lm}(\hat{\boldsymbol{k}})\, Y_{lm}(\hat{\boldsymbol{r}}), \tag{A.1}$$

where the $j_l(kr)$ are the spherical Bessel functions. Without loss of generality we now consider only the CLO's centred on position $\boldsymbol{q}$ and we drop the index $\boldsymbol{q}$ in the Dirac brackets. Using the expansion and Eq. (10) gives for the CLO–PW overlap matrix element

$$\langle nlm|\boldsymbol{k}\rangle = \frac{1}{\sqrt{V_{\mathrm{ws}}}} \int_{V_{\mathrm{ws}}} e^{i\boldsymbol{k}\boldsymbol{r}} \sum_{\boldsymbol{R}} e^{-(i\boldsymbol{k}\boldsymbol{R})} \times \tilde{\phi}^*_{nlm}(\boldsymbol{r} - \boldsymbol{q} - \boldsymbol{R})\, d\boldsymbol{r}. \tag{A.2}$$

Integration is only over a single Wigner–Seitz cell near the origin, leaving only the $\boldsymbol{R} = 0$ term. We prefer now, to make the following choice:

$$\Psi_{nlm}(r, \theta, \phi) = f_{nl}(r)\, Y_{lm}(\theta, \phi). \tag{A.3}$$

Using further Eq. (A.1) one obtains

$$\begin{aligned}
\langle nlm|\boldsymbol{k}\rangle &= \frac{1}{\sqrt{V_{\mathrm{ws}}}} \int_{V_{\mathrm{ws}}} e^{i\boldsymbol{k}\boldsymbol{r}} f_{nl}(|\boldsymbol{r} - \boldsymbol{q}|)\, Y^*_{lm}(\theta, \phi)\, d\boldsymbol{r} \\
&= \frac{4\pi}{\sqrt{V_{\mathrm{ws}}}} e^{i\boldsymbol{k}\boldsymbol{q}} \sum_{l'=0}^{\infty} i^{l'} \sum_{m'=-l'}^{l'} Y^*_{l'm'}(\hat{\boldsymbol{k}}) \\
&\quad \times \int_0^{R_c} j_{l'}(kr) f_{nl}(r) r^2\, dr \int_{4\pi} Y_{l'm'}(\hat{\boldsymbol{r}})\, Y^*_{lm}(\hat{\boldsymbol{r}})\, d\hat{\boldsymbol{r}} \\
&= \frac{4\pi}{\sqrt{V_{\mathrm{ws}}}} e^{i\boldsymbol{k}\boldsymbol{q}} \sum_{l'=0}^{\infty} i^{l'} \sum_{m'=-l'}^{l'} Y^*_{l'm'}(\hat{\boldsymbol{k}}) \\
&\quad \times \int_0^{R_c} j_{l'}(kr) f_{nl}(r) r^2\, dr\, \delta_{ll',mm'} \\
&= \frac{4\pi}{\sqrt{V_{\mathrm{ws}}}} e^{i\boldsymbol{k}\boldsymbol{q}}\, i^l\, Y^*_{lm}(\hat{\boldsymbol{k}}) \int_0^{R_c} j_l(kr) f_{nl}(r) r^2\, dr.
\end{aligned} \tag{A.4}$$

This expression becomes Eq. (13) after substituting $\boldsymbol{k} + \boldsymbol{g}$ for $\boldsymbol{k}$ and $\tilde{R}_{nl}(r)$ for $f_{nl}(r)$.

For the Hamiltonian matrix elements we assume in this paper (conform the ASA approach) that $V(\boldsymbol{r}) = V(r)$. We use Green's theorem (the integrals over the sphere surface are zero) and obtain for the CLO–CLO Hamiltonian matrix elements:

$$\begin{aligned}
&\langle nlm|H|n'l'm'\rangle \\
&= \frac{1}{2} \int_0^{R_c} r^2 \left(\frac{d\tilde{R}_{nl}}{dr}\right)\left(\frac{d\tilde{R}_{n'l}}{dr}\right) dr\, \delta_{ll',mm'} \\
&\quad + \int_0^{R_c} \left[\frac{l(l+1)}{2r^2} + V(r)\right] r^2 \tilde{R}_{nl}(r)\, \tilde{R}_{n'l}(r)\, dr\, \delta_{ll',mm'} \\
&= \int_0^{R_c} \left[\frac{1}{2}\left[r^2 \left(\frac{d\tilde{R}_{nl}}{dr}\right)\left(\frac{d\tilde{R}_{n'l}}{dr}\right) \right.\right. \\
&\qquad \left. + l(l+1)\, \tilde{R}_{nl}(r) \tilde{R}_{n'l}(r)\right] \\
&\qquad \left. + V(r) r^2 \tilde{R}_{nl}(r)\, \tilde{R}_{n'l}(r)\right] dr\, \delta_{ll',mm'},
\end{aligned} \tag{A.5}$$

which is the result Eq. (16). Nonspherical corrections to the potential can easily be added. The delta function in the integral over the potential is replaced in this case by a Gaunt integral.

Remains the derivation of the CLO–PW Hamiltonian matrix element, the last one left. This is quite easy, if one makes use of the fact that

$$\left[-\frac{\nabla^2}{2} + V(r) \right] |\boldsymbol{k}\rangle = [\tfrac{1}{2}k^2 + V(r)]|\boldsymbol{k}\rangle. \tag{A.6}$$

All we have to do now is to use at Eq. (A.4) the choice for f:

$$f_{nl}(r) = [\tfrac{1}{2}k^2 + V(r)]\,\tilde{R}_{nl}(r), \tag{A.7}$$

and to substitute $\boldsymbol{k} \to \boldsymbol{k} + \boldsymbol{g}$, to obtain immediately the result Eq. (17). Nonspherical corrections to the potential can in this case be added in the same way as previously mentioned.

References

[1] C. Herring, Phys. Rev. 57 (1940) 1169.
[2] J.C. Slater, Phys. Rev. 51 (1937) 151.
[3] S.G. Louie, K.M. Ho and M.L. Cohen, Phys. Rev. B 19 (1979) 1774.
[4] M.H. Kang, R.C. Tatar, E.J. Mele and P. Soven, Phys. Rev. B 35 (1987) 5457.
[5] D.J. Singh, H. Krakauer, C. Haas and A.Y. Liu, Phys. Rev. B 46 (1992) 13065.
[6] C.M.J. Wijers, G.P.M. Poppe, P.L. de Boeij, H.G. Bekker and D.J. Wentink, Thin Solid Films 233 (1993) 28.
[7] R.P. Feynman, Phys. Rev. 56 (1939) 340.
[8] P. Pulay, Mol. Phys. 17 (1969) 197.
[9] R. Yu, D. Singh and H. Krakauer, Phys. Rev. B 43 (1991) 6411.
[10] B.H. Bransden and C.J. Joachain, Physics of Atoms and Molecules (Longman, London/New York, 1986).
[11] O.K. Andersen, Phys. Rev. B 12 (1975) 3060.
[12] E.C. Snow, Phys. Rev. 158 (1967) 683.
[13] J.S. Faulkner, Phys. Rev. 178 (1969) 914.
[14] P. Modrak, Phys. Rev. B 46 (1992) 15716, Table 3.
[15] G.A. Burdick, Phys. Rev. 129 (1963) 138.
[16] T. Takeda and J. Kübler, J. Phys. F: Metal Phys. 9 (1979) 661.
[17] O.K. Andersen, Z. Pawlowska and O. Jepsen, Phys. Rev. B 34 (1986) 5253.